J. Ocean Univ. China (Oceanic and Coastal Sea Research)
https://doi.org/10.1007/s11802-022-4811-y
ISSN 1672-5182, 2022 21 (1): 15-27
http://www.ouc.edu.cn/xbywb/
E-mail:xbywb@ouc.edu.cn

Analysis of Wave Distributions Using the WAVEWATCH-III Model in the Arctic Ocean

SHAO Weizeng[1), 2), *], YU Wupeng[1)], JIANG Xingwei[2), 3)], SHI Jian[4)], WEI Yongliang[5)], and JI Qiyan[1), *]

1) *Marine Science and Technology College*, *Zhejiang Ocean University*, *Zhoushan* 316000, *China*
2) *National Satellite Ocean Application Service*, *Beijing* 100081, *China*
3) *Southern Marine Science and Engineering Guangdong Laboratory*, *Guangzhou* 511458, *China*
4) *College of Meteorology and Oceanography*, *National University of Defense Technology*, *Nanjing* 211101, *China*
5) *College of Marine Sciences*, *Shanghai Ocean University*, *Shanghai* 201306, *China*

(Received October 20, 2020; revised November 26, 2020; accepted December 8, 2020)

Abstract In this work, we examined long-term wave distributions using a third-generation numerical wave model called WAVEWATCH-III (WW3) (version 6.07). We also evaluated the influence of sea ice on wave simulation by using eight parametric switches. To select a suitable ice-wave parameterization, we validated the simulations from the WW3 model in March, May, September, and December 2017 against the measurements from the Jason-2 altimeter at latitudes of up to 60°N. Generally, all parameterizations exhibited slight differences, *i.e.*, about 0.6 m root mean square error (RMSE) of significant wave height (SWH) in May and September and about 0.9 m RMSE for the freezing months of March and December. The comparison of the results with the SWH from the European Centre for Medium-Range Weather Forecasts for December 2017 indicated that switch IC4_M1 performed most effectively (0.68 m RMSE) at high latitudes (60°–80°N). Given this finding, we analyzed the long-term wave distributions in 1999–2018 on the basis of switch IC4_M1. Although the seasonal variability of the simulated SWH was of two types, *i.e.*, 'U' and 'sin' modes, our results proved that fetch expansion prompted the wave growth. Moreover, the interannual variability of the specific regions in the 'U' mode was found to be correlated with the decade variability of wind in the Arctic Ocean.

Key words long-term wave distribution; sea ice; WAVEWATCH-III; Arctic Ocean

1 Introduction

Owing to global climate change, gradual reductions in the area, thickness, and quantity of perennial sea ice in the Arctic Ocean during the summer have been occurring since the late 1990s (Shimada *et al.*, 2006; Kawaguchi *et al.*, 2012). Under these circumstances, sea ice reduction enhances the intensity of Arctic waves (Thomson and Rogers, 2014) as the available sea fetch broadens (Dobson *et al.*, 1989), resulting in conditions that are conducive to the growth of swells (Thomson and Rogers, 2014). A string of broken ice floes floats on the sea surface when waves propagate in a sea ice shelf, and it is likely to be distorted by wind and ocean currents, thus effectively enhancing the heat exchange in the sea atmospheric layer (Kohout *et al.*, 2014).

The interaction between sea ice and ocean waves is an interesting scientific topic, although it has remained a complex issue because sea ice affects ocean waves by scattering and dissipating wave energy (Squire *et al.*, 1995; Squire *et al.*, 2009). Specifically, wave energy does notdissipate instantaneously upon encountering ice-covered sea (Tolman, 2003). On the contrary, ocean waves can penetrate the sea ice cover, where their amplitude significantly attenuates (Cheng *et al.*, 2017); hence, wave energy diffuses to the inner region of sea ice covers. In recent years, a number of studies have revealed a correlation between ocean waves and the splitting, location, and melting of sea ice in polar regions. In particular, ocean waves penetrate the entire ice cover near the ice edge, thereby forming a region known as the marginal ice zone (MIZ), where waves penetrate into the ice and huge ice layers smash to a few floes at tens of meters (Doble and Bidlot, 2013). The MIZ is an important area between the open ocean and internal floating ice where ocean waves, sea ice, and the atmosphere strongly interact.

Since 1940, observational data concerning ocean wave attenuation in sea ice has been quantitatively recorded (Wadhams, 1973). With the awareness of rapid sea ice reduction in polar seas, a few studies have investigated ice-wave interactions under continuous projects, *e.g.*, the Greenland Arctic Shelf Ice and Climate Experiment (Green-

* Corresponding authors.
E-mail: shaoweizeng@mail.tsinghua.edu.cn
E-mail: jiqiyan@zjou.edu.cn

ICE) (Wadhams *et al.*, 2004) and the Boundary Layer Physics of the Emerging Arctic Ocean (SeaState) field campaign conducted from 30 September to 4 November 2015. Remotely sensed data, *e.g.*, synthetic aperture radar data, are also valuable sources for studying the wave properties of ice-covered waters (Wadhams and Holt, 1991; Wadhams *et al.*, 2002; Wadhams, 2004). The two issues that need to be solved to determine the influence of sea ice on waves are wave attenuation/dispersion of frequency (Squire and Moore, 1980; Wadhams *et al.*, 1988) and the scattering of directional wave energy (Wadhams *et al.*, 1986). The theoretical models for wave propagation in ice-covered waters include the pure viscous layer model (Carolis and Desiderio, 2002), elastic plate model (Kohout and Meylan, 2008), viscoelastic model (Wang and Shen, 2010; Squire and Montiel, 2016), and thin elastic plate scattering model (Williams *et al.*, 2013).

The third-generation numerical wave model WAVEWATCH-III (WW3) is a well-known model used for global wave simulation (Mondon and Warner, 2009; Bi *et al.*, 2015; Zheng *et al.*, 2015). It includes the parameterizations of theoretical models (WAVEWATCH-III Development Group, 2019) and thus provides alternative modules to describe ice-wave effects. The eight available parameterizations are IC1, IC2, IC3, IC4_M1, IC4_M2, IC5, IS1, and IS2. The performance of these models, however, should be investigated on the basis of varying ice thicknesses and concentrations.

The remainder of this manuscript is organized as follows. Section 2 briefly describes the relevant datasets, including the wind forcing data for the WW3 model, as well as the ice data and measurements from the Jason-2 altimeter. Section 3 describes the alternative parameterizations. Section 4 provides the validation results from which the best parameterization is selected so as to analyze the long-term wave distributions in the Arctic Ocean from 1999 to 2018. Section 5 presents the discussion. Section 6 summarizes the conclusions.

2 Description of Dataset

The dataset consists of three types of data: 1) the forcing data from the open-access European Centre for Medium-Range Weather Forecasts (ECMWF); 2) the sea ice data for the ice-wave modules in the WW3 model; 3) the measurements from the Jason-2 altimeter for validating the simulated significant wave heights (SWHs).

2.1 Forcing Data and Model Settings

Since 1979, the ECMWF has continuously provided global atmospheric-oceanic products for investigators at intervals of six hours each day (Molteni *et al.*, 2010). Although the wind and wave parameters, *i.e.*, wind vectors and combined wind-sea and swell, can be openly accessed from the ECMWF-interim (ERA) datasets, individual wind-sea and swell data are not available. Thus, this information cannot be applied to long-term wave distribution analysis. ERA wind is a reliable resource serving as the forcing field for wave simulation using the WW3 model; in particular, it was employed in our previous studies on typhoon wave simulations (Shao *et al.*, 2018; Sheng *et al.*, 2019). In the current study, the 0.125° gridded wind vectors at 00:00, 06:00, 18:00, and 24:00 UTC were utilized as the forcing field. As an example, the ERA wind map of the Arctic Ocean at 12:00 on 17 May 2017 is shown in Fig.1 for wind speeds $<22\,\mathrm{m\,s^{-1}}$.

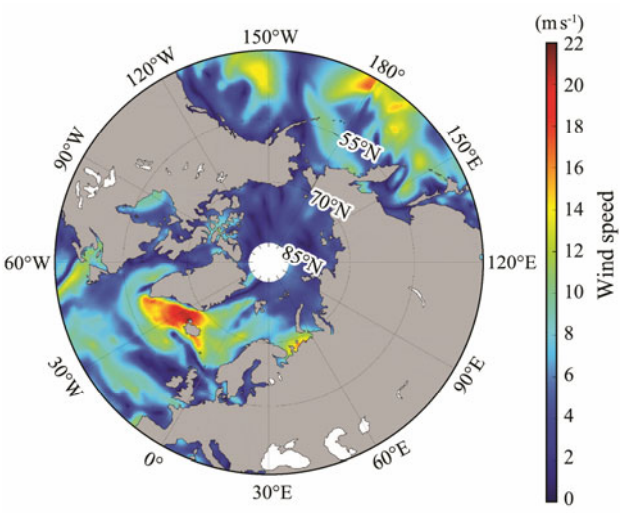

Fig.1 Wind map from the European Centre for Medium-Range Weather Forecasts (ECMWF)-interim (ERA) of the Arctic Ocean at 12:00 UTC on 17 May 2017.

The simulated region at the MIZ in the Arctic Ocean was set to 40°–85°N latitude and 0°–360°E longitude, and the bathymetric topography with 30 arc-second intervals (about 1 km horizontal resolution) from GEBCO was used. The model ran from 1 January 1999 to 30 December 2018. In studying the performance of eight ice-wave parameterizations, the outputs on a 0.25° grid in March, May, September, and December 2017 were validated against the measurements from the Jason-2 altimeter. The default settings of the WW3 model were utilized and are listed in Table 1. Among the switches, the input/dissipation source terms using the parametric ST2 package (Sheng *et al.*, 2019) and the quadruplet wave-wave interactions, denoted as the GMD2 package (Shao *et al.*, 2018), were artificially selected.

Table 1 Settings of the WAVEWATCH-III (WW3) model

Parameter	Setting
Frequency bins	The frequency bins ranged logarithmically from 0.04118 to 0.7186 at an interval of $\Delta f/f = 0.1$
Spatial propagation	300 s time steps in the longitudinal and latitudinal directions
Resolution	0.5° grid with 60 min temporal resolution
Spectrum setting	The two-dimensional wave spectrum was resolved into 24 regular azimuthal directions with a 15° step; outputs included individual wind-sea and swell

2.2 Ice Data

The sea ice concentration and ice thickness data from the Copernicus Marine Environment Monitoring Service (CMEMS) were available for the ice-wave modules from 1993 to 2018. The maps of average sea ice concentration and thickness for September 2017 respectively shown in Figs.2a and 2b were chosen as an example because sea ice begins to melt in early May and supposedly reaches the minimum in September, decreasing at a rate of −8.6%± 2.9% per decade (Duan *et al.*, 2019). The spatial coverage of sea ice extends south to 70˚N. Figs.2c and 2d present the anomalies of sea ice concentration and thickness, respectively, in September 1998 to 2018. Sea ice thickness gradually decreased starting in 2006, with a maximum annual reduction of approximately 0.55 m in 2012. Moreover, sea ice concentration significantly changed, diminishing by more than 16% in September 2012. Although sea ice expands in December, with the spatial coverage extending to 55˚N, sea ice thickness was thinnest in 2012 (Fig.3). Collectively, the data on sea ice concentration and thickness were taken as the forcing field in the wave simulation from the WW3 model with consideration of the ice-wave interaction term.

2.3 Wave Data from Jason-2 Altimeter

Given the few observations from moored buoys in the Arctic Ocean, measurements from the Jason-2 altimeter are a reliable source for wave climate studies (Liu *et al.*, 2016), although the latitude of the available data from the Jason-2 altimeter only extends poleward as far as 60˚N. Therefore, in this study, the wave data from the Jason-2 altimeter for the months of March, May, September, and December 2017 were collected. Note that because the time difference between the measurements from the Jason-2 altimeter and the simulations from the WW3 model was within 30 min, the output was set to 60 min. In sum, we compiled more than 10000 match-ups with the simulations from the WW3 model for each month. Fig.4 shows a wave map using the WW3 model in the Arctic Ocean at

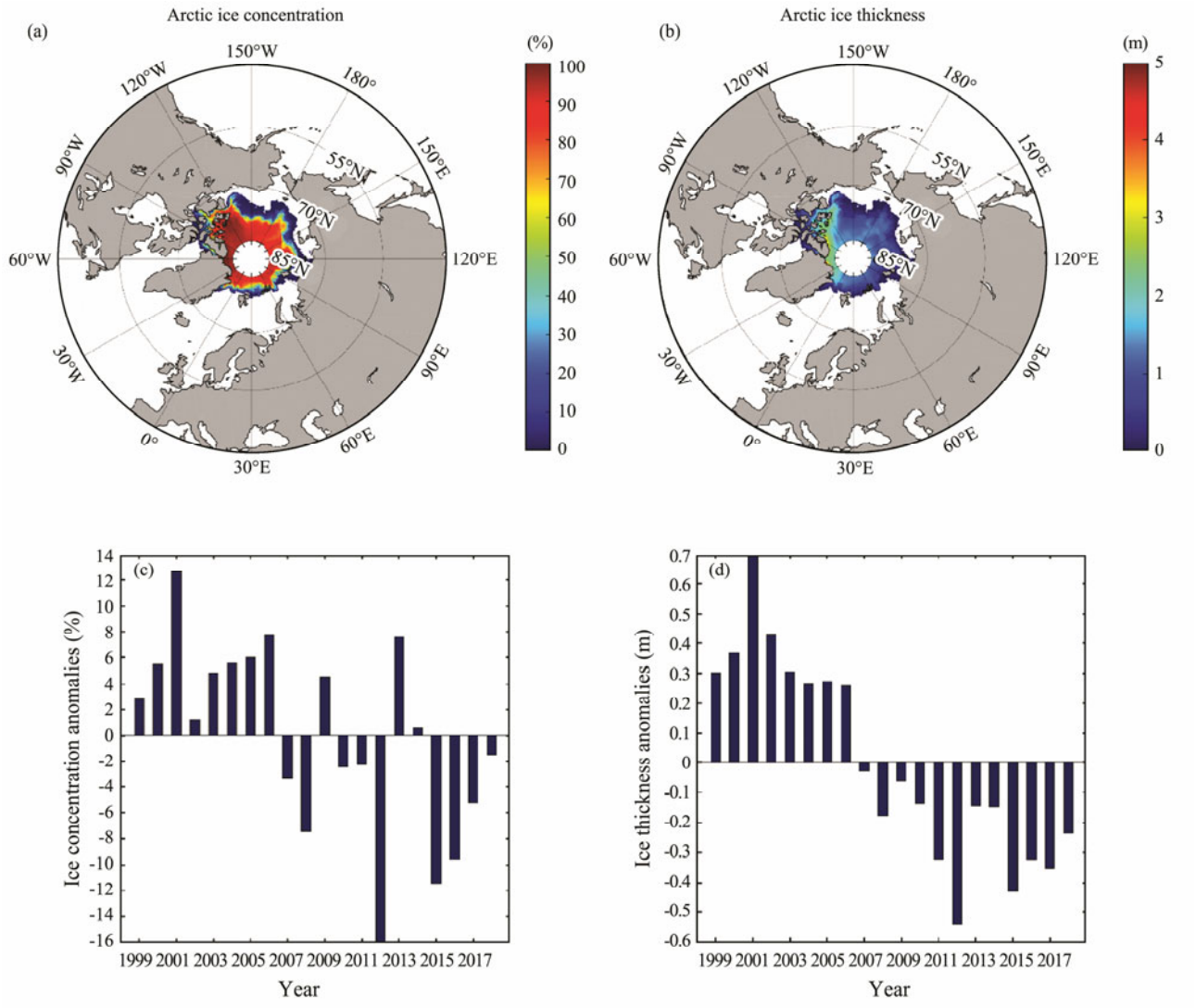

Fig.2 (a), Maps of average sea ice concentration in September 2017; (b), maps of average sea ice thickness in September 2017; (c), anomalies of sea ice concentration in September 1998 to 2018; (d), anomalies of sea ice thickness in September 1998 to 2018.

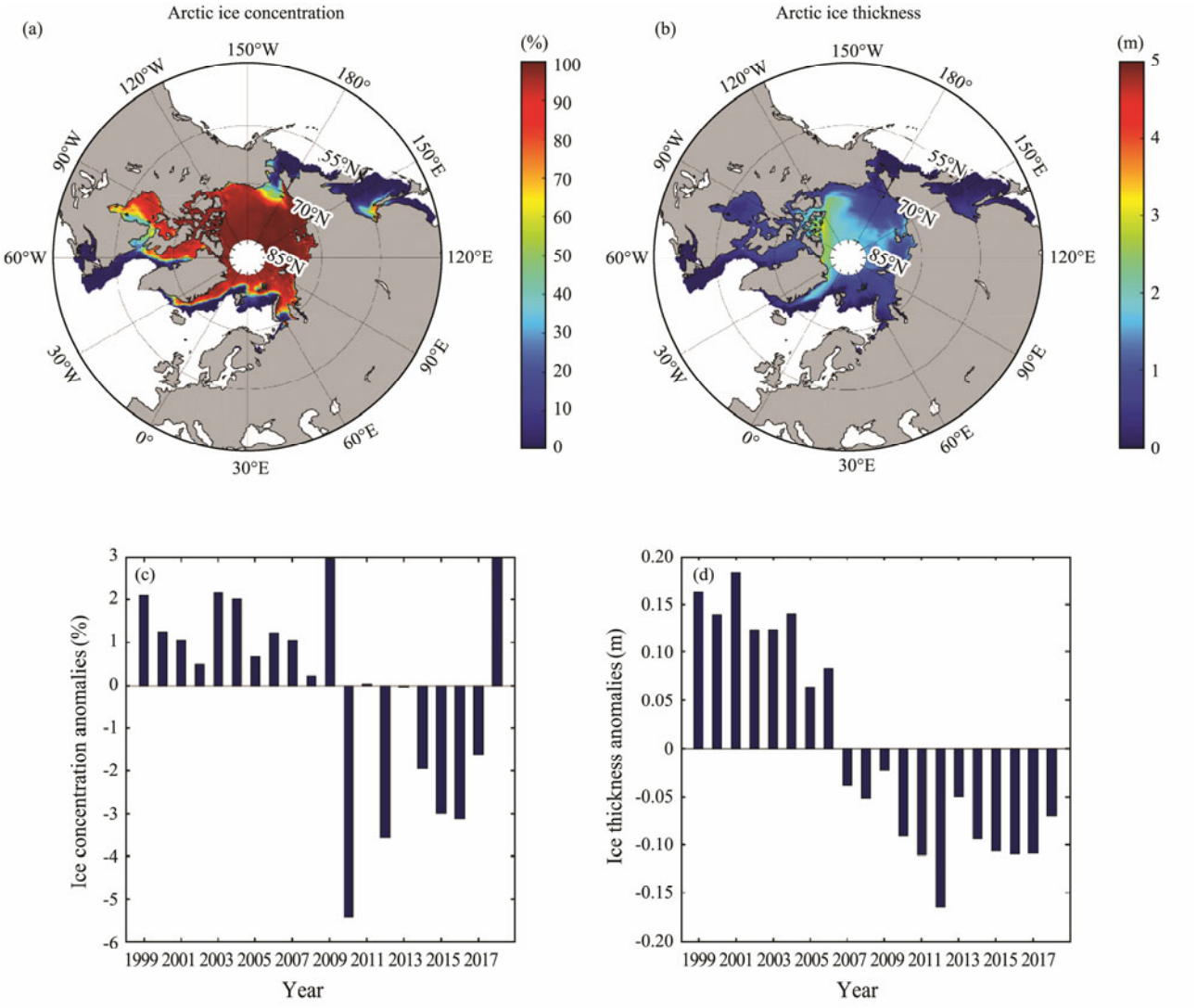

Fig.3 (a), Maps of average sea ice concentration in December 2017; (b), maps of average sea ice thickness in December 2017; (c), anomalies of sea ice concentration in December 1998 to 2018; (d), anomalies of sea ice thickness in December 1998 to 2018.

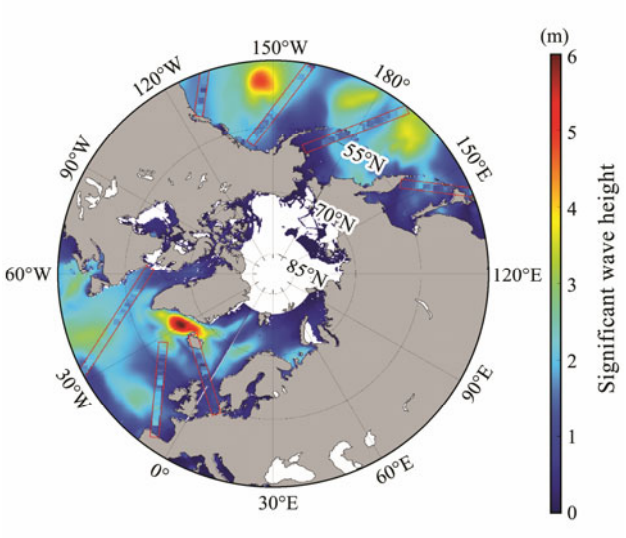

Fig.4 Wave map using the WW3 model of the Arctic Ocean at 12:00 UTC on 17 May 2017, overlaid by the footprints (red rectangles) of the Jason-2 altimeter from 06:00 to 18:00.

12:00 on 17 May 2017, overlaid by the footprints (red rectangles) of the Jason-2 altimeter from 06:00 to 18:00. The measurements from the Jason-2 altimeter were consistent with the patterns from the WW3-simulated SWHs. Hence, we concluded that the simulation from the WW3 model were suitable for this study. To investigate the performance of each ice-wave term at high latitudes ranging from 60˚N to 85˚N, we also directly employed the ERA wave fields for the four months in 2017.

3 Methodology

The wave propagation equation of the WW3 model is given as

$$\frac{\partial N}{\partial t}+\frac{\partial C_x N}{\partial x}+\frac{\partial C_y N}{\partial y}+\frac{\partial C_\sigma N}{\partial \sigma}+\frac{\partial C_\theta N}{\partial \theta}=\frac{S}{\sigma}, \qquad (1)$$

where the prognostic variable represents the wave action density spectrum N expressed as a function of space (x and y), time t, and wave direction θ and is equal to the

energy density E divided by the angular relative frequency σ ($N=E/\sigma$); C_x and C_y are the wave action propagation speeds in the x- and y-spaces, respectively. In the absence of currents, C_x is the x-component of group velocity C_g. The right-hand side of the governing equation is determined by the rate of change of wave action density $S(x, y, \sigma, \theta, t)$, which is generally represented by three terms, *i.e.*, the input term from the sea surface wind, nonlinear interactions, and dissipation (Sheng *et al.*, 2019).

Sea ice generally modifies the wavelength/wave-number and dissipation rate of wind-generated ocean waves (Liu *et al.*, 1991). The ice-modified wave-number can be expressed as a complex number $k=k_r+ik_i$. The real part, k_r, represents the effect of sea ice on the physics of wave propagation, *e.g.*, shoaling and refraction by the change of water depth. The imaginary part, $k_i(x, y, \sigma, t)$, is produced by the wave represented by the attenuation exponential decay coefficient $S_{\text{ice}}/E=-2C_gk_i$; it can be introduced in a wave model such as the WW3, where S_{ice} is one dissipation term on the right-hand side of the governing equation. At present, the WW3 model (version 6.07) provides parametric source terms and includes the five dissipation parameters of ocean wave energy (IC1–IC5). In addition, the reflection and scattering of ocean waves induced by sea ice follow the conservative processes without dissipation (Wadhams, 1975), which are treated separately in switches IS1 and IS2 (WAVEWATCH-III Development Group, 2019).

3.1 IC Switch Terms

This method involves the utilization of five ice parameters, $C_{\text{ice},1}-C_{\text{ice},5}$: $C_{\text{ice},1}$ is used for ice thickness (m); $C_{\text{ice},2}$ for viscosity ($\text{m}^2\,\text{s}^{-1}$); $C_{\text{ice},3}$ for density ($\text{kg}\,\text{m}^{-3}$); $C_{\text{ice},4}$ for the effective shear modulus (Pa); and $C_{\text{ice},5}$ for mean diameter floes (m). Moreover, additional information on ice concentration, *ICE*, is taken as a unique forcing field.

The first switch implementation method (IC1) assumes the imaginary part, $C_{\text{ice},1}=k_i$, excluding other parameters. In this case, $C_{\text{ice},1}$ is taken as the unsteady value of a forcing field using ice thickness. Switch IC2 is a method for expressing wave energy dissipation through wave-ice interaction (Liu and Mollo-Christensen, 1988), in which the main input ice parameter is the ice thickness $C_{\text{ice},1}$ that varies spatially and temporally. Recently, switch IC2 has been improved by the addition of a good alternative to the eddy viscosity representation of dissipation. In the improved version, the ice-induced dissipation transmits from a laminar form using molecular viscosity multiplied by an adjustment factor to a turbulent form for Reynolds numbers above an empirical threshold (Stopa *et al.*, 2016). In our work, the settings were made following the suggestions of Stopa *et al.* (2016). Switch IC3, which is determined by ice-wave interactions and was obtained from Wang and Shen (2010), is a vortex viscosity model that treats sea ice as a viscoelastic layer, with a dispersion relation associated with σ and k. Switch IC3 requires four parameters, $C_{\text{ice},1}-C_{\text{ice},4}$. Technically, $C_{\text{ice},1}$ is the unsteady value of a forcing field, and $C_{\text{ice},2-4}=[0.03, 917, 0]$.

The original purpose of switch IC4 was to provide the empirical function describing the high-frequency wave attenuation in the MIZ observed by Wadhams *et al.* (1988). This method parameterizes the well-known low-pass filtering effect of ice and is expressed as follows:

$$\alpha=\exp\left(\frac{-2\pi C_{\text{ice},1}}{\sigma}-C_{\text{ice},2}\right), \tag{2}$$

where α is the exponential decay rate for energy treated as twice that of the amplitude, *i.e.*, $\alpha=2k_i$. The other two variables, $C_{\text{ice},1}$ and $C_{\text{ice},2}$, tuned from the dataset are equal to 0.18 and 7.3, respectively. The above method is denoted as IC4_M1 in this manuscript. The coefficients of the fourth-degree polynomial using a flexible method for prescribed attenuation were proposed by Meylan *et al.* (2014), with the wave attenuation data measured in the Antarctic Ocean. The polynomial function appears to be proportional to the wave-number at low frequency attenuation, whereas high-frequency waves require high-order attenuation rates with strongly nonlinear dependence, denoted as IC4_M2.

$$\alpha=C_{\text{ice},1}+C_{\text{ice},2}\left(\frac{\sigma}{2\pi}\right)+C_{\text{ice},3}\left(\frac{\sigma}{2\pi}\right)^2+C_{\text{ice},4}\left(\frac{\sigma}{2\pi}\right)^3+C_{\text{ice},5}\left(\frac{\sigma}{2\pi}\right)^4, \tag{3}$$

where the default values for the coefficients are $C_{\text{ice},1-5}=[0, 0, 2.12\times10^{-3}, 0, 4.59\times10^{-2}]$.

The fifth method, IC5, for representing ice-induced wave decay is based on another viscoelastic-type model, *i.e.*, the EFS ice layer model described in Mosig *et al.* (2015). This type of approach introduces viscosity into the thin elastic plate model and restricts it to one horizontal dimension; here, the plate is replaced with a beam. The dispersion relation given by the EFS model is expressed in the following form:

$$\sigma^2=Qgk\tanh(kd), \tag{4}$$

where

$$Q=\frac{G_\eta h_i^3}{6\rho_\omega g}(1+\nu)k^4-\frac{\rho_i h_i\sigma^2}{\rho_\omega g}+1, \tag{5}$$

$$G_\eta=G-i\sigma\rho_i\eta, \tag{6}$$

in which G is the effective elastic shear modulus, η is the effective viscosity, ρ_ω is the density of water, ρ_i is the density of sea ice, d is the water depth, h_i is the ice cover thickness, σ is the angular relative frequency, $k=k_r+ik_i$ is the complex wave-number, g is the gravitational acceleration, and ν is a constant equal to 0.3 and refers to the Poisson ratio of sea ice. Similar to switch IC3, switch IC5 requires four parameters taken as inputs: $C_{\text{ice},1}$ for ice thickness h_i (m), $C_{\text{ice},2}$ for effective viscosity η ($\text{m}^2\,\text{s}^{-1}$), $C_{\text{ice},3}$ for ice density ρ_i ($\text{kg}\,\text{m}^{-3}$), and $C_{\text{ice},4}$ for effective shear modulus G (Pa). Similar to IC3, $C_{\text{ice},1}$ is also set as a

forcing field, and $C_{\text{ice},2\text{–}4}$ = [5.0E+7, 917.0, 4.9E+12].

3.2 IS Switch Terms

The conservative effect of sea ice on wave propagation is implemented in switch IS1 and represents a simple mechanism of scattering as waves encounter sea ice. The size of ice floes is assumed to be smaller than the grid, resulting in a fraction α_{ice} of the incoming wave energy being scattered isotropically. The fraction α_{ice} is determined from sea ice concentration by using a simple linear transfer function:

$$\alpha_{\text{ice}} = \max\{0, C_1 + C_2\}. \quad (7)$$

The coefficients C_1 and C_2 are customizable through the name list SIS1, with the name list parameters ISC1 = 1.0×10^{-2} and ISC2 = -0.2×10^{-2} (WAVEWATCH-III Development Group, 2019). At each discrete frequency and in each discrete direction, the wave energy is reduced by the amount of α_{ice} and redistributed in all directions at the same discrete frequency to conserve energy propagation.

The parameterization method in switch IS2 is an improved scattering model (Moon *et al.*, 2007). Principally, the implementation of this scattering term includes an estimation of the sea ice breakup induced by waves, an approach that can consider sea ice with large floe diameters. The scattering source term is defined by the scattering coefficient $\beta_{\text{is,MIZ}}$ and is expressed as follows:

$$\frac{S_{\text{is}}(k,\theta)}{\sigma} = \int_0^{2\pi} \beta_{\text{is,MIZ}}(\theta,\theta')[S_{\text{scat}} N(k,\theta') - N(k,\theta)]\mathrm{d}\theta, \quad (8)$$

where S_{scat} is set to the default value of 1, θ is the wave direction, and θ' is the wave direction after scattering. The determination of the scattering coefficient $\beta_{\text{is,MIZ}}$ is based on the theoretical reflection coefficient $\alpha_n(\sigma, C_{\text{ice},1})$ under the hypothesis that waves usually propagate from a half-plane of open water to a half-plane of ice-covered water with a constant ice thickness $C_{\text{ice},1}$. Excluding multiple reflections, the scattering coefficient $\beta_{\text{is,MIZ}}$ is parametric and defined as the successor attenuation for each floe of a mean diameter D_m with a partial reflection $\alpha_n(\sigma, C_{\text{ice},1})$ due to broken ice. Thus, the coefficient is treated as a series of ice-water interfaces:

$$\beta_{\text{is,MIZ}} = C_i C_g \alpha_n(\sigma, C_{\text{ice},1}) / D_m, \quad (9)$$

in which c_i is the ice concentration ICE and $D_m = 500$ (WAVEWATCH-III Development Group, 2019).

The settings of the eight switches used in the ice-wave modules are listed in Table 2.

Table 2 Settings used in the ice-wave modules of the WW3 model

Switch ID	$C_{\text{ice},1}$	$C_{\text{ice},2}$	$C_{\text{ice},3}$	$C_{\text{ice},4}$	$C_{\text{ice},5}$	U_{10}	*ICE*
IC1	Forcing field	–	–	–	–	Forcing field	Forcing field
IC2	Forcing field	1536.0E−4	–	–	–	Forcing field	Forcing field
IC3	Forcing field	0.03	917	0	–	Forcing field	Forcing field
IC4_M1	Forcing field	7.3	–	–	–	Forcing field	Forcing field
IC4_M2	Forcing field	0	2.12E−3	0	4.59E−2	Forcing field	Forcing field
IC5	Forcing field	5.0E+7	917	4.9E+12	–	Forcing field	Forcing field
IS1	–	–	–	–	–	Forcing field	Forcing field
IS2	Forcing field	–	–	–	500	Forcing field	Forcing field

4 Results

Before investigating the short-term analysis of wave distribution in the Arctic Ocean, the best parameterization of ice-wave interaction in the WW3 model should be selected. We first present the average wave maps using switch IC3 in the Arctic Ocean in four months of 2017, *i.e.*, March (Fig.5a), May (Fig.5b), September (Fig.5c), and December (Fig.5d). The average SWHs in March and December were as high as 5 m, whereas those in May and September were relatively low for the region south of 60°N. This type of behavior is inconsistent with the average SWH being larger in May and September because of the expansion of fetch that results in the sufficient growth of ocean waves. We believe that multiple factors, *e.g.*, wind, sea ice concentration, sea thickness, and regional sea characteristics, determine the waves in the Arctic Ocean; these factors are explored in a later section. Fig.6 shows the validation of SWH against measurements from the Jason-2 altimeter using switch IC3 in September 2017 (a) and December 2017 (b). WW3 performed well, *i.e.*, the root mean square error (RMSE) for SWH was about 0.6 m and the correlation (Cor) was 0.89 in May with the reduction of sea ice while the RMSE for SWH was about 0.9 m and the Cor was 0.87 in December with the expansion of sea ice. Similar findings were revealed by the statistical analysis using eight switches (Table 3). All parameterizations exhibited slight SWH differences in May and September when the sea ice was contracting relative to those in the two freezing months of March and December when the sea ice was expanding.

The ERA wave fields in December 2017 at latitudes of 60°–85°N were used to confirm the accuracy of the SWHs simulated using the eight ice-wave modules. Fig.7 shows the average ECMWF wave map (a) and the simulated wave maps using three switches: IC4_M1 (b), IS1 (c), and IS2 (d) in December. Although wave patterns were clearly observed using the three switches and were consistent with the waves from the ECMWF, the waves were missed when IS1 and IS2 were used, *e.g.*, in region (70°–80°N, 120°E–120°W). In contrast to the ECMWF wave pattern, the wave pattern (SWH > 3 m) was cut off crossing the panel at [0°N, 60°N] using those switches.

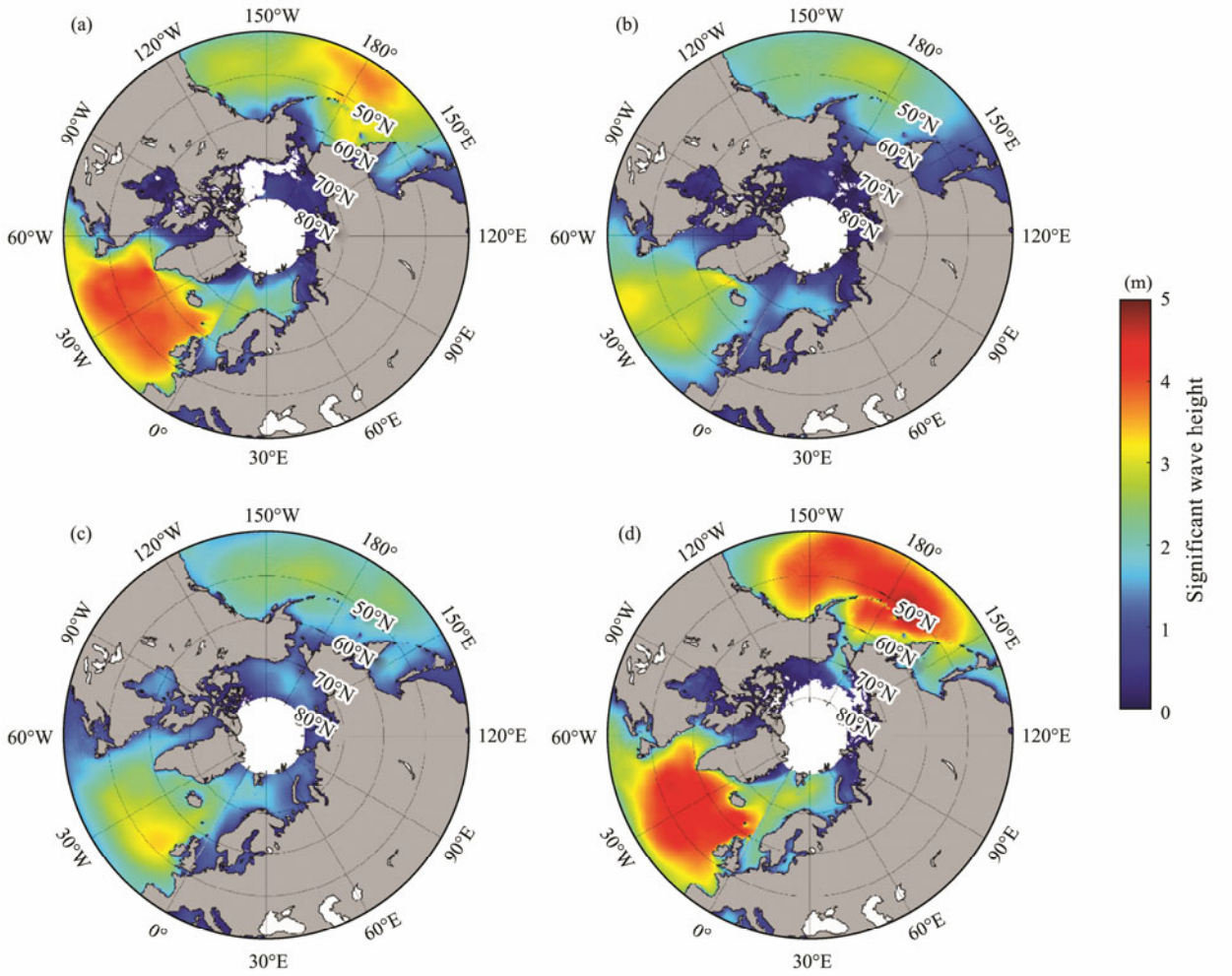

Fig.5 Average wave maps using the WW3 model of the Arctic Ocean in four months of 2017 using switch IC3: (a), March; (b), May; (c), September; (d) December.

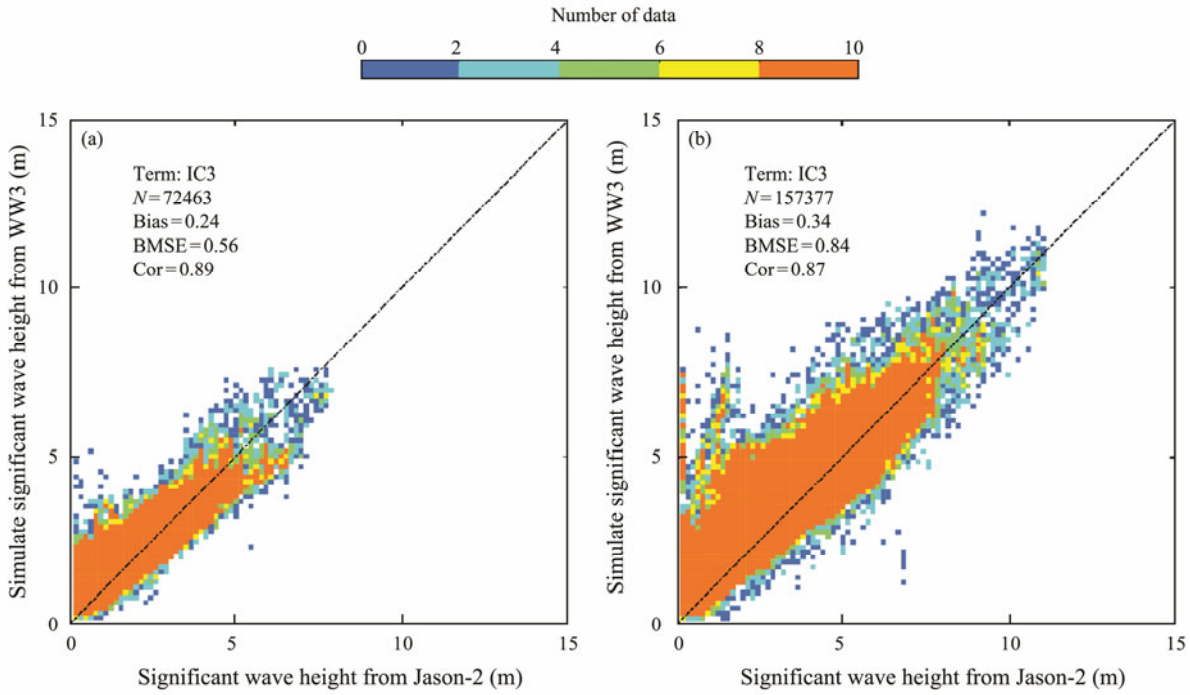

Fig.6 Comparison with significant wave heights from the Jason-2 altimeter up to 60˚N using the IC3 ice-wave terms in (a) September 2017 and (b) December 2017.

Table 3 Statistical analysis using eight switches

Switch ID	Month	Bias (m)	RMSE (m)	Correlation	Scatter index
IC1	May	0.53	1.00	0.81	0.27
	March	0.17	0.58	0.85	0.25
	September	0.21	0.54	0.89	0.26
	December	0.44	0.96	0.85	0.25
IC2	May	0.48	0.93	0.83	0.25
	March	0.17	0.57	0.85	0.25
	September	0.21	0.54	0.89	0.26
	December	0.39	0.88	0.86	0.23
IC3	May	0.44	0.90	0.84	0.25
	March	0.16	0.56	0.85	0.25
	September	0.21	0.54	0.89	0.26
	December	0.34	0.84	0.87	0.23
IC4_M1	May	0.46	0.91	0.83	0.25
	March	0.16	0.57	0.86	0.26
	September	0.21	0.55	0.90	0.27
	December	0.36	0.85	0.87	0.23
IC4_M2	May	0.52	0.99	0.81	0.27
	March	0.17	0.57	0.85	0.25
	September	0.21	0.54	0.89	0.26
	December	0.43	0.95	0.85	0.25
IC5	May	0.45	0.90	0.83	0.25
	March	0.16	0.56	0.85	0.25
	September	0.21	0.55	0.90	0.26
	December	0.35	0.85	0.87	0.23
IS1	May	0.43	0.89	0.83	0.25
	March	0.15	0.56	0.85	0.25
	September	0.21	0.54	0.89	0.26
	December	0.33	0.83	0.87	0.22
IS2	May	0.44	0.90	0.83	0.25
	March	0.15	0.57	0.85	0.26
	September	0.21	0.55	0.89	0.25
	December	0.34	0.84	0.87	0.23

The results of the statistical analysis of the ECMWF SWH in December using eight switches are presented in Table 4. We believe that IC4_M1 exhibited superior performance (0.68 m SWH) because of the wave simulation deficiencies while using IS1 and IS2.

Table 4 Statistical analysis using eight switches in December 2017

Switch ID	Bias (m)	RMSE (m)	Correlation	Scatter index
IC1	0.84	1.08	0.83	0.26
IC2	0.71	0.91	0.86	0.26
IC3	0.52	0.69	0.89	0.17
IC4_M1	0.53	0.68	0.90	0.16
IC4_M2	0.85	1.09	0.83	0.26
IC5	0.57	0.74	0.89	0.18
IS1	0.36	0.49	0.92	0.13
IS2	0.49	0.62	0.91	0.15

5 Discussion

In this section, we further examine the long-term analysis of wave distribution from 1998 to 2018. Fig.8 shows the RMSE, scatter index (SI), Bias (ECMWF minus WW3), and Cor for the collocated SWHs with ERA waves using switch IC4_M1. A relatively large error (>0.5 m RMSE) occurred in the region (60°–70°N, 0°–5°E), as indicated by the black rectangle. This error was probably caused by the two aspects of using switch IC4_M1: the cutting off effect crossing the region at [0°N, 60°N] and the underestimation of bias of up to 1.5 m. This inferior performance should be improved in the future when using the WW3 model for wave simulations in the Arctic Ocean.

The expanse of the Arctic Ocean at latitudes above 60°N was manually divided into the following eight major regions to examine the characteristics of wave distribution: Hudson Bay, Baffin Bay, Greenland Sea, Iceland, Norwegian Sea, Barents Sea, Kara Sea, and Chukchi Sea (Fig.9). The seasonal variability of sea ice concentration, ECMWF wind speed, sea ice thickness, and WW3-simulated SWH for those eight regions in 2017 are presented in Fig.10. As shown in Fig.10d, the seasonal variability could be divided into two types: 'U' mode, which includes the Greenland Sea, Iceland, the Norwegian Sea, and the Barents Sea; and 'sin' mode, which includes the Kara Sea, Baffin Bay, Hudson Bay, and the Chukchi Sea. We focused on the variability from May to October, during which the ECMWF wind decreased. As for the 'U' mode, the SWH decreased from May to June and then increased until October. This type of behavior confirmed the effect of the expansion of fetch on wave growth, especially during the rapid reduction of sea ice. By contrast, the SWH in the 'sin' mode is highly sensitive to the reduction of sea ice

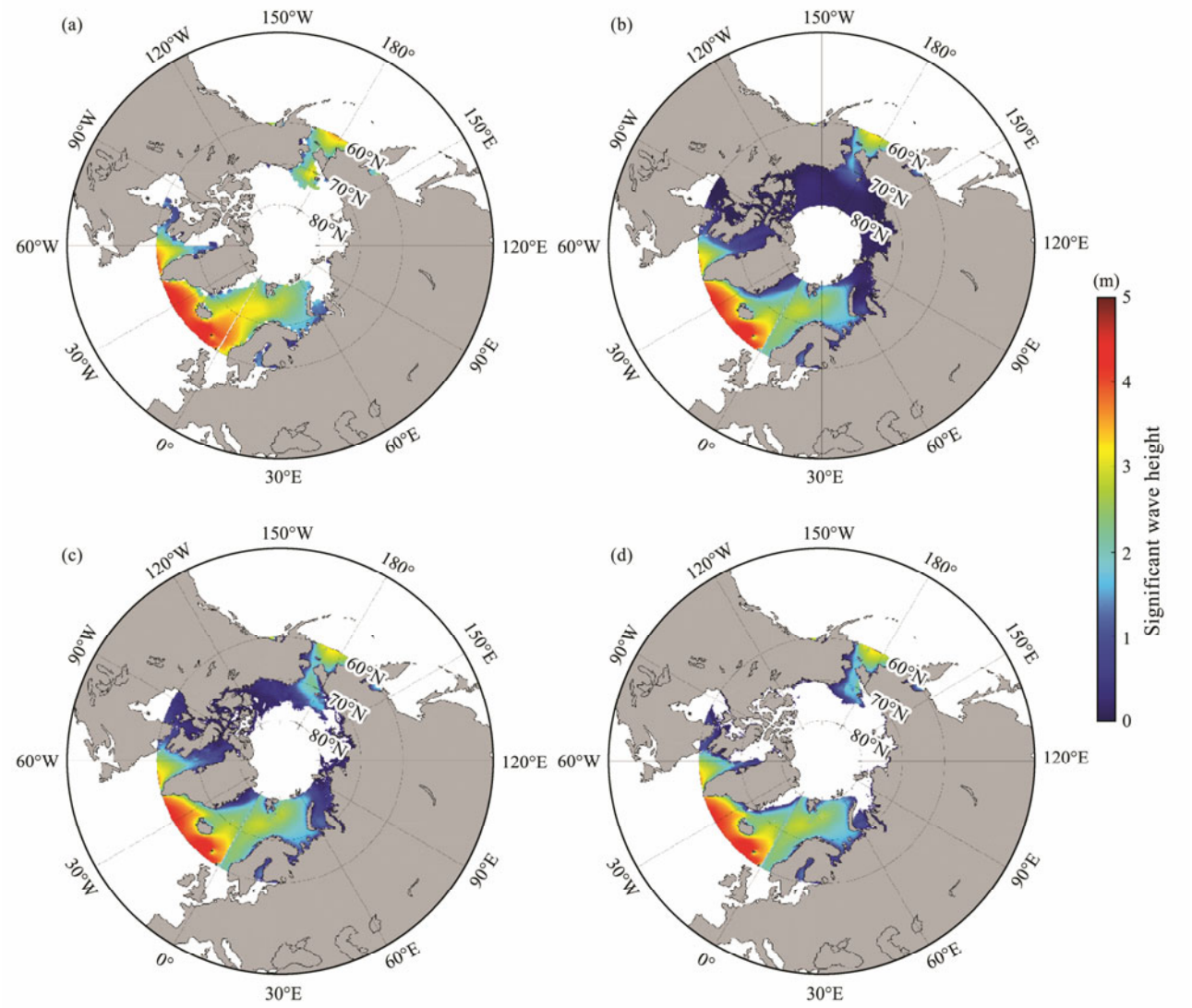

Fig.7 Average ECMWF wave map and simulated wave maps using two switches at latitudes in the range of 60˚–85˚N in December: (a), ECMWF; (b), IC_M1; (c), IS1; (d) IS2.

because the SWH grows as the wind speed decreases. The continuous interannual variability during the period of 1999–2018 is plotted in Fig.11. Two apparent peaks were identified in 2011 and 2015 in the regions previously in the 'U' mode (marked by ellipses in Figs.11b and 11d, respectively), although the annual series of SWHs exhibited no clear tendency with the other variables. Therefore, we believe that the decade variability of wind is largely responsible for the interannual variability of waves in the Arctic Ocean.

6 Conclusions

The anomalies indicated that the sea coverage experienced its largest reduction in 2012; this observation is consistent with the findings of a previous study (Duan *et al.*, 2019). Against the backdrop of sea ice reduction, an enhanced wave climate is anticipated because of the large areas of open ocean. At present, the wave climate in the Arctic Ocean is a topic worth exploring for the oceanography community. In this study, the long-term wave distributions in the Arctic Ocean 1999–2018 were analyzed using the latest WW3 model (version 6.07). In particular, the characteristics of specific regions were examined in great detail.

Ice-wave interactions are important considerations in wave simulations of the Arctic Ocean. In this study, we investigated the applicability of eight switches provided by the WW3 model (version 6.07) with consideration of the influence of ice-wave mechanisms in the Arctic Ocean. The eight switches were denoted as IC1, IC2, IC3, IC4_M1, IC4_M2, IC5, IS1, and IS2; and ERA wind, CMEMS sea ice concentration, and CMEMS were taken as the forcing fields. First, the simulations on a 0.25˚ grid from the WW3 model for March, May, September, and December 2017 were validated against the available measurements from the Jason-2 altimeter for latitudes of up to 60˚N. The comparisons revealed an RMSE of about 0.6 of the SWH in May and September during the reduction of sea ice and an RMSE of about 0.9 m in March and December during the expansion of sea ice. Second, the simulations were compared with the ERA waves at high latitudes in the

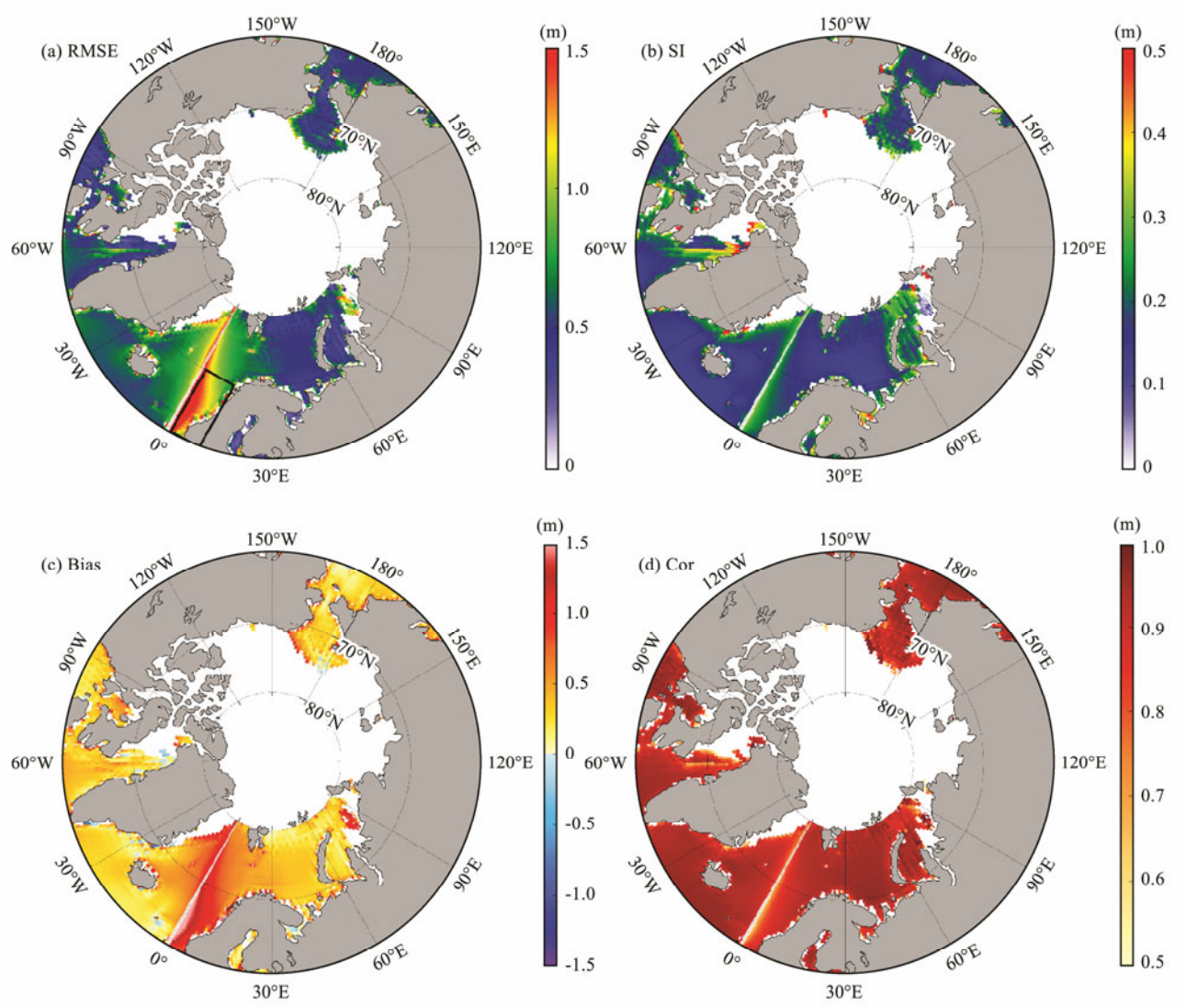

Fig.8 Statistical analysis for the collocated SWHs and ERA waves using switch IC4_M1 from 1998 to 2018: (a), root mean square error (RMSE); (b), scatter index (SI); (c), Bias (ECMWF minus WW3); (d) correlation (Cor).

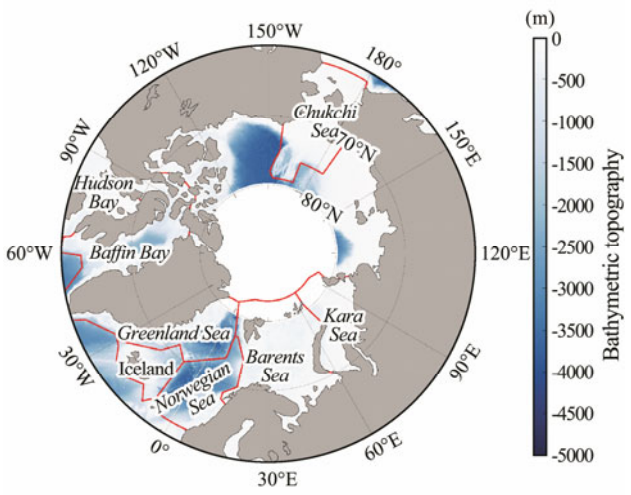

Fig.9 Eight major regions extracted from the Arctic Ocean.

range of 60°–80°N. Although the RMSE of the SWH was 0.49 m when switch IS1 was used, switch IC4_M1 was found to be more suitable for wave simulation (RMSE= 0.68 m) because of the wave simulation deficiencies while using switches IS1 and IS2 at high latitudes.

We divided the distribution of the Arctic Ocean at latitudes above 60°N into eight specific regions. The seasonal variability of sea ice concentration, ECMWF wind speed, sea ice thickness, and WW3-simulated SWH in 2017 indicated two modes, namely, the 'U' and 'sin' modes. In the 'U' mode, the SWH troughs appeared in June. In the 'sin' mode, the SWH gradually increased with decreasing wind speed in May until October probably because of the expansion of fetch associated with the reduction of sea ice. The interannual wave variability revealed that the wind speed trend was consistent with the SWH in the 'U' mode. In particular, two crests occurred in 2011 and 2015, although no clear correlation of SWH with other variables was found in the 'sin' mode.

The reduction of sea ice should enhance the fetch in the Antarctic Ocean as well. In the future, the applicability of the WW3 model to the Antarctic Ocean will be investigated, and the climatology of Antarctic circumpolar waves will then be analyzed.

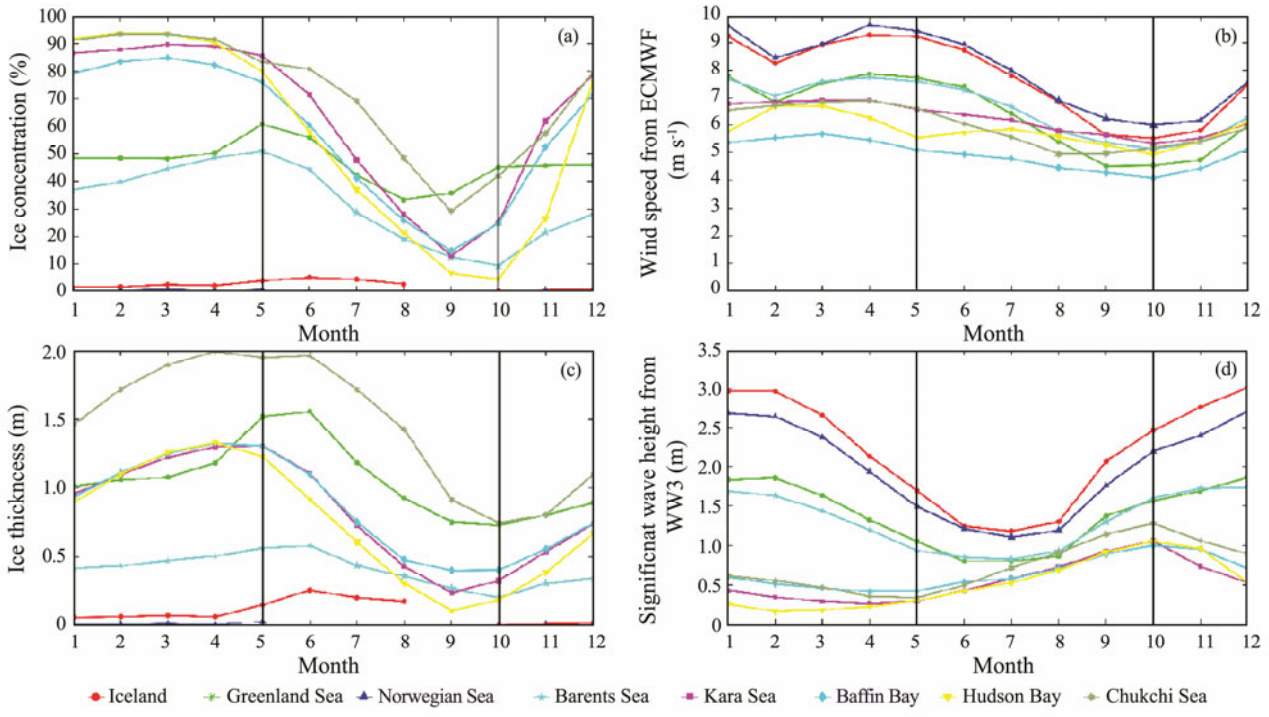

Fig.10 Seasonal variations of (a), sea ice concentration; (b), ECMWF wind speed; (c), sea ice thickness; and (d), WW3-simulated SWH for specific regions of the Arctic Ocean in 2017.

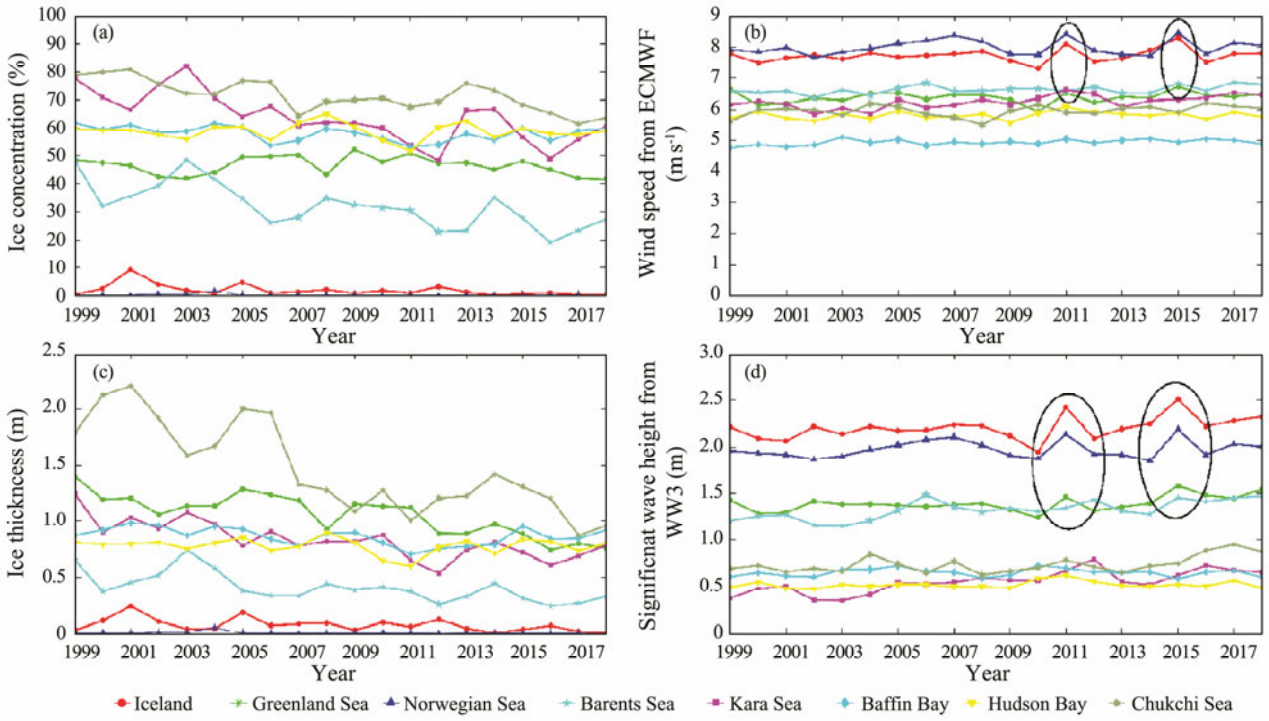

Fig.11 Interannual variabilities of (a), sea ice concentration; (b), ECMWF wind speed; (c), sea ice thickness; and (d), WW3-simulated SWH for specific regions of the Arctic Ocean during the period of 1999–2018.

Acknowledgements

The authors acknowledge support from the National Key Research and Development Program of China (No. 2016 YFC1401605), the Key Special Project for Introduced Talents Team of Southern Marine Science and Engineering Guangdong Laboratory (Guangzhou) (No. GML2019ZD 0302), and the National Natural Science Foundation of China (Nos. 41806005 and 42076238). We appreciate the provision of the National Centers for Environmental Prediction of the National Oceanic and Atmospheric Administration of the source code of the WAVEWATCH-III (WW3) model, which they supplied for free. We also thank the European Centre for Medium-Range Weather Forecasts for providing the interim wind data on a 0.125° grid, which can

be openly downloaded from http://www.ecmwf.int. The water depth data from the General Bathymetric Chart of the Oceans were collected from ftp.edcftp.cr.usgs.gov, and the Operational Geophysical Data Record wave data from the Jason-2 altimeter mission were accessed *via* https://data.nodc.noaa.gov. In addition, we would like to thank the Copernicus Marine Environment Monitoring Service for offering sea ice concentration and thickness data as forcing fields for the WW3 model, which we obtained free of charge from http://marine.copernicus.eu.

References

Bi, F., Song, J. B., Wu, K. J., and Xu, Y., 2015. Evaluation of the simulation capability of the Wavewatch III model for Pacific Ocean wave. *Acta Oceanologica Sinica*, **34** (9): 43-57.

Carolis, G. D., and Desiderio, D., 2002. Dispersion and attenuation of gravity waves in ice: A two-layer viscous fluid model with experimental data validation. *Physics Letters A*, **305** (6): 399-412.

Cheng, S. K., Erick, R. W., Jim, T., Smith, M., Doble, M. J., Wadhams, P., Kohout, A. L., Lund, B., Persson, O. P. G., Collons, C. O., Ackley, S. F., Montiel, F., and Shen, H. H., 2017. Calibrating a viscoelastic sea ice model for wave propagation in the Arctic fall marginal ice zone. *Journal of Geophysical Research: Oceans*, **122** (11): 8770-8793.

Doble, M. J., and Bidlot, J. R., 2013. Wave buoy measurements at the Antarctic sea ice edge compared with an enhanced ECMWF WAM: Progress towards global waves-in-ice modelling. *Ocean Modelling*, **70**: 166-173.

Dobson, F., Perrie, W., and Toulany, B., 1989. On the deep-water fetch laws for wind-generated surface gravity waves. *Atmosphere Ocean*, **27** (1): 210-236.

Duan, C. L., Dong, S., Xie, Z. X., and Wang, Z. F., 2019. Temporal variability and trends of sea ice in the Kara Sea and their relationship with atmospheric factors. *Polar Science*, **20**: 136-147.

Kawaguchi, Y., Hutchings, J. K., Kikuchi, T., Morison, J. H., and Krishfield, R. A., 2012. Anomalous sea-ice reduction in the Eurasian Basin of the Arctic Ocean during summer 2010. *Polar Science*, **6**: 39-53.

Kohout, A. L., and Meylan, M. H., 2008. An elastic plate model for wave attenuation and ice floe breaking in the marginal ice zone. *Journal of Geophysical Research Oceans*, **113** (C9): 1-17.

Kohout, A. L., Williams, M. J. M., Dean, S. M., and Meylan, M. H., 2014. Storm-induced sea-ice breakup and the implications for ice extent. *Nature*, **509** (7502): 604-607.

Liu, A. K., and Mollo-Christensen, E., 1988. Wave propagation in a solid ice pack. *Journal of Physical Oceangraphy*, **18** (11): 1702-1712.

Liu, A. K., Holt, B., and Vachon, P. W., 1991. Wave propagation in the marginal ice zone: Model predictions and comparisons with buoy and synthetic aperture radar data. *Journal of Geophysical Research*, **96** (C3): 4605-4621.

Liu, Q. X., Alexander, V. B., Stefan, Z., Young, L. R., and Guan, C. L., 2016. Wind and wave climate in the Arctic Ocean as observed by altimeters. *Journal of Climate*, **29** (22): 7957-7975.

Meylan, M. H., Bennets, L., and Kohout, L. A., 2014. *In situ* measurements and analysis of ocean waves in the Antarctic marginal ice zone. *Geophysical Research Letters*, **41** (14): 5046-5051.

Molteni, F., Buizza, R., Palmer, T. N., and Petroliagis, T., 2010. The ECMWF ensemble prediction system: Methodology and validation. *Quarterly Journal of the Royal Meteorological Society*, **122** (529): 73-119.

Mondon, E., and Warner, P., 2009. Synthesis of a validated nearshore operational wave database using the archived NOAA Wave Watch III ocean model data and SWAN nearshore model. *10th International Coastal Symposium (ICS 2009)*. Lisbon, Portugal, 1015-1019.

Moon, I. J., Ginis, I., Hara, T., and Thomas, B., 2007. A physics-based parameterization of air-sea momentum flux at high wind speeds and its impact on hurricane intensity predictions. *Monthly Weather Review*, **135** (8): 2869-2878.

Mosig, J. E. M., Montiel, F., and Squire, V. A., 2015. Comparison of viscoelastic-type models for ocean wave attenuation in ice-covered seas. *Journal of Geophysical Research: Oceans*, **120** (9): 6072-6090.

Shao, W. Z., Sheng, Y. X., Li, H., Shi, J., Ji, Q. Y., Tan, W., and Zou, J. C., 2018. Analysis of wave distribution simulated by WAVEWATCH-III model in typhoons passing Beibu Gulf, China. *Atmosphere*, **9** (7): 265-284.

Sheng, Y. X. Shao, W. Z., Li, S. Q., Zhang, Y. M., Yang, H. W., and Zou, J. C., 2019. Evaluation of typhoon waves simulated by WaveWatch-III model in shallow waters around Zhoushan islands. *Journal of Ocean University of China*, **18** (2): 365-375.

Shimada, K., Kamoshida, T., Itoh, M., Nishino, S., Carmack, E., Mclaughlin, F., Zimmermann, S., and Proshutinshy, A., 2006. Pacific Ocean inflow: Influence on catastrophic reduction of sea ice cover in the Arctic Ocean. *Geophysical Research Letters*, **33** (8): 153-172.

Squire, V. A., and Montiel, F., 2016. Evolution of directional wave spectra in the marginal ice zone: A new model tested with legacy data. *Journal of Physical Oceanography*, **46** (10): 3121-3137.

Squire, V. A., and Moore, S. C., 1980. Direct measurement of the attenuation of ocean waves by pack ice. *Nature*, **283** (5745): 365-368.

Squire, V. A., Dugan, J. P., Wadhams, P., Rottier, P. J., and Liu, A. K., 1995. Of ocean waves and sea ice. *Annual Reviews of Fluid Mechanics*, **27** (1): 115-168.

Squire, V. A., Vaughan, G. L., and Bennetts, L., 2009. Ocean surface wave evolvement in the Arctic Basin. *Geophysical Research Letters*, **36** (22): L22502.

Stopa, J. E., Fabrice, A., and Fanny, G. A., 2016. Wave climate in the Arctic 1992–2014: Seasonality and trends. *The Cryosphere*, **10** (4): 1605-1629.

Thomson, J., and Rogers, W. E., 2014. Swell and sea in the emerging Arctic Ocean. *Geophysical Research Letters*, **41** (9): 1-6.

Tolman, H. L., 2003.Treatment of unresolved islands and ice in wind wave models. *Ocean Modelling*, **5** (3): 219-231.

Wadhams, P., 1973. Attenuation of swell by sea ice. *Journal of Geophysical Research Atmospheres*, **78** (18): 3552-3563.

Wadhams, P., 1975. Airborne laser profiling of swell in an open ice field. *Journal of Geophysical Research*, **80** (33): 4520-4528.

Wadhams, P., 2004. SAR imaging of wave dispersion in Antarctic pancake ice and its use in measuring ice thickness. *Geophysical Research Letters*, **31** (15): 305-316.

Wadhams, P., and Holt, B., 1991. Waves in frazil and pancake ice and their detection in seasat synthetic aperture radar imagery. *Journal of Geophysical Research Oceans*, **96** (C5): 8835-8852.

Wadhams, P., Doble, M. J., Toudal, L., Gudmansen, P., Mikkelsen, N., Haas, C., Gill, R. S., and Forsberg, R., 2004. Greenland ice and climate experiment (GreenICE). *Monash Bioethics Review*, **24** (3): 62-6.

Wadhams, P., Parmiggiani, F., and De Carolis, G., 2002. The use of SAR to measure ocean wave dispersion in Frazil-Pancake icefields. *Journal of Physical Oceanography*, **32** (6): 1721-1746.

Wadhams, P., Squire, V. A., Ewing, J. A., and Pascal, R. W., 1986. The effect of the marginal ice zone on the directional wave spectrum of the ocean. *Journal of Physical Oceanography*, **16** (2): 358-376.

Wadhams, P., Squire, V. A., Goodman, D. J., Cowan, A. M., and Moore, S. C., 1988. The attenuation rates of ocean waves in the marginal ice zone. *Journal of Geophysical Research*, **93** (C6): 6799-6818.

Wang, R. X., and Shen, H. H., 2010. Gravity waves propagating into an ice-covered ocean: A viscoelastic model. *Journal of Geophysical Research*, **115** (C6): 1-12.

WAVEWATCH III Development Group, 2019. User manual and system documentation of WAVEWATCH III version 6.07. NOAA Tech. Note MMAB Contribution 333, Camp Springs, National Oceanic and Atmospheric Administration, US.

Williams, T. D., Bennetts, L. G., Squire, A. V., Dumont, D., and Bertino, L., 2013. Wave-ice interactions in the marginal ice zone. Part 1: Theoretical foundations. *Ocean Model*, **71** (9): 81-91.

Zheng, K. W., Sun, J., Guan, C. L., and Shao, W. Z., 2015. Analysis of the global swell and wind sea energy distribution using WAVEWATCH III. *Advances in Meteorology*, **2016** (7): 1-9.

(Edited by Xie Jun)